HHS Public Access

Author manuscript

J Comp Neurol. Author manuscript; available in PMC 2020 February 15.

Published in final edited form as:

J Comp Neurol. 2019 February 15; 527(3): 546–557. doi:10.1002/cne.24451.

Morphological heterogeneity among corticogeniculate neurons in ferrets: quantification and comparison with a previous report in macaque monkeys

J. Michael Hasse[1,2,3], **Elise M. Bragg**[4], **Allison J. Murphy**[5], and **Farran Briggs**[1,2,3]

[1]Ernest J. Del Monte Institute for Neuroscience, University of Rochester School of Medicine, Rochester NY 14642 USA

[2]Department of Neuroscience, University of Rochester School of Medicine, Rochester NY 14642 USA

[3]Center for Visual Science, University of Rochester, Rochester NY 14642 USA

[4]Department of Psychiatry, Dartmouth-Hitchcock Medical Center, Lebanon NH 03756 USA

[5]Neuroscience Graduate Program, University of Rochester, Rochester NY 14642 USA

Abstract

The corticogeniculate (CG) pathway links the visual cortex with the lateral geniculate nucleus (LGN) of the thalamus and is the first feedback connection in the mammalian visual system. Whether functional connections between CG neurons and LGN relay neurons obey or ignore the separation of feedforward visual signals into parallel processing streams is not known. Accordingly, there is some debate about whether CG neurons are morphologically heterogeneous or homogenous. Here we characterized the morphology of CG neurons in the ferret, a visual carnivore with distinct feedforward parallel processing streams, and compared the morphology of ferret CG neurons with CG neuronal morphology previously described in macaque monkeys (Briggs et al, 2016). We used a G-deleted rabies virus as a retrograde tracer to label CG neurons in adult ferrets. We then reconstructed complete dendritic morphologies for a large sample of virus-labeled CG neurons. Quantification of CG morphology revealed three distinct CG neuronal subtypes with striking similarities to the CG neuronal subtypes observed in macaques. These findings suggest that CG neurons may be morphologically diverse in a variety of highly visual mammals in which feedforward visual pathways are organized into parallel processing streams. Accordingly, these results provide support for the notion that CG feedback is functionally parallel stream-specific in ferrets and macaques.

Corresponding Author: Farran Briggs, Ph.D., University of Rochester School of Medicine, 601 Elmwood Ave., Box 603, Rochester, NY 14642, Phone: (585) 276-3736, farran_briggs@urmc.rochester.edu, Fax: (585) 756-5334.

CONFLICT OF INTEREST

None of the authors on this study have any real or potential conflict of interest that could inappropriately influence this study.

ROLE OF AUTHORS

All of the authors had full access to all of the data in this study and take responsibility for the integrity of the data and the accuracy of the data analyses. J.M.H., E.M.B., and F.B. conceived of and designed the study. E.M.B., J.M.H. completed the neuronal reconstructions. J.M.H. and A.J.M. analyzed the data. J.M.H., A.J.M., and F.B. and wrote the manuscript.

Graphical Abstract

Corticogeniculate neurons in the ferret visual cortex are morphologically diverse. Illustrated here are images and overlaid reconstructions of corticogeniculate neurons in areas 17 and 18, with short, tilted, stellate, tall-tufted, and displaced morphologies. Black lines indicate laminar boundaries and scale bar applies to all images and reconstructions.

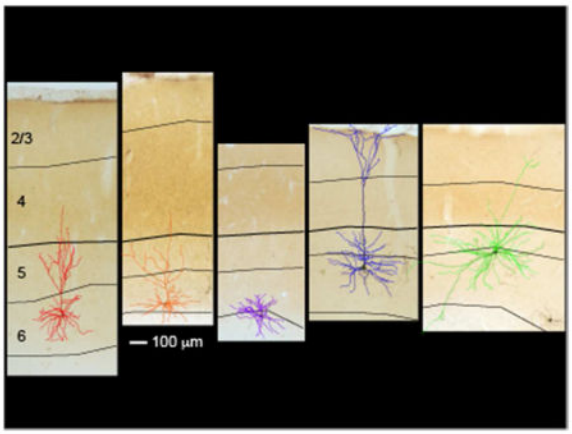

Keywords

corticogeniculate; V1; LGN; morphology; RRID: AB_10013483; RRID: AB_221570; RRID: SCR_001775; RRID: SCR_001622

INTRODUCTION

Visual information traverses feedforward circuits from the retina through the lateral geniculate nucleus (LGN) of the thalamus to the visual cortex. The first feedback connection in the mammalian visual system is the corticogeniculate (CG) pathway linking visual cortex to the LGN (Jones 1985, Sherman & Guillery 2006). In highly visual mammals, such as carnivores and primates, feedforward visual circuits are organized into parallel information processing streams (Casagrande & Xu 2004). Parvocellular, magnocellular, and koniocellular streams convey signals about visual form/acuity, motion, and color in primates; homologous X, Y, and W streams constitute the feedforward pathways in carnivores (Callaway 2004, Kaplan 2004, Sherman & Guillery 2006). Physiological evidence suggests that CG feedback is also organized into parallel streams that align with the feedforward streams (Briggs & Usrey 2009). However, direct evidence indicating functional stream-specificity among CG circuits is lacking. Alternatively, it is possible that parallel organization of CG circuits is a primate specialization. Here we examined morphological diversity among CG neurons in ferrets, highly visual carnivores with distinct feedforward parallel streams (Jackson & Hickey 1985), and compared CG morphology in ferrets and macaque monkeys to determine whether distinct CG neuronal subtypes are similar across species.

The CG pathway is anatomically robust in that CG synapses onto LGN relay neurons far outnumber retinal synapses (Erisir et al 1997a, Erisir et al 1997b, Guillery 1969, Sherman &

Guillery 2006). However, the functional impact of CG feedback on the activity of individual LGN neurons is subtle. Rather than alter the receptive field physiology of LGN neurons, CG feedback reduces the response latency and variability of LGN neurons, effectively sharpening the temporal and spatial resolution of LGN responses to incoming visual inputs (Andolina et al 2013, Andolina et al 2007, Hasse & Briggs 2017). Physiological recordings from CG neurons in carnivores and primates reveal multiple physiologically distinct CG subtypes, separated based on axon conduction latency (Briggs & Usrey 2005, Briggs & Usrey 2007, Grieve & Sillito 1995, Harvey 1978, Tsumoto & Suda 1980). In macaques, CG subtypes defined based on axon conduction latency also display physiological response properties that align precisely with the feedforward parvocellular, magnocellular, and koniocellular streams (Briggs & Usrey 2009). Although physiological evidence in carnivores and primates hints at parallel stream organization for CG feedback, morphological evidence for parallel stream organization across species is mixed, and no direct link between physiologically and morphologically distinct CG neuronal subtypes has been made.

A number of morphological properties of CG neurons are similar across mammals. CG neurons are all excitatory neurons with cell bodies restricted to cortical layer 6 (Briggs et al 2016, Brumberg et al 2003, Conley & Raczkowski 1990, Fitzpatrick et al 1994, Katz 1987, Usrey & Fitzpatrick 1996). Most CG neurons reside in primary visual cortex (V1 or area 17) with a smaller population of CG neurons in secondary visual cortex (V2 or area 18) (Briggs et al 2016, Gilbert & Kelly 1975, Lin & Kaas 1977, Murphy et al 2000, Updyke 1975). Based on dendritic arborization patterns, most CG neurons fall into two broad morphological classes: short and tall pyramidal neurons. Short CG neurons have dendrites that target layers 4 and 5, but not more superficial layers, while tall CG neurons have dendrites extending into layer 2/3 (Briggs 2010). Short and tall CG neurons appear to form distinct CG neuronal subtypes in cats (Gilbert & Kelly 1975, Katz 1987), while rodent CG neurons fall along a continuum from short-like to tall-like with less evidence for morphologically distinct CG subtypes (Brumberg et al 2003, Jiang et al 1993). In contrast, macaque CG neurons display a number of unique morphological specializations (Briggs et al 2016).

Unlike in cats and rodents where CG cell bodies are distributed throughout the depth of layer 6 (Gilbert & Kelly 1975, Katz 1987), primate CG cell bodies are segregated into sub-tiers within layer 6 (Briggs et al 2016, Conley & Raczkowski 1990, Fitzpatrick et al 1994). This sub-laminar organization for CG neuronal cell bodies likely reflects the axonal termination patterns for collaterals of geniculocortical inputs (Blasdel & Lund 1983, Hendrickson et al 1978, Hubel & Wiesel 1972). Specifically, CG neurons projecting to parvocellular and more dorsal koniocellular layers of the LGN reside in the top tier of layer 6, which is also the termination zone for parvocellular geniculocortical collaterals (Fitzpatrick et al 1994). CG neurons projecting to magnocellular and more ventral koniocellular LGN layers reside in the bottom tier of layer 6, the termination zone for magnocellular geniculocortical collaterals (Fitzpatrick et al 1994).

CG neurons in macaques also display greater morphological diversity compared to other species. An extensive study of macaque CG neurons that employed viral tracing methods enabling broad sampling of CG neurons, including rare neuronal types, revealed at least 5

distinct morphological subtypes of CG neurons in V1 (Briggs et al 2016). Many CG neurons were short (Iβ) or tall (IC) as described previously (Briggs & Callaway 2001, Wiser & Callaway 1996). Additional morphological subtypes included stellate, tilted, and large CG neurons. All of the morphological subtypes described displayed strict sub-laminar segregation, with cell bodies located either in the top or bottom tiers of layer 6, consistent with prior results (Conley & Raczkowski 1990, Fitzpatrick et al 1994, Usrey & Fitzpatrick 1996). Interestingly, results of a thorough study of CG neuronal morphology in galagos (*Otolemer garnettii*) suggested little morphological diversity among CG neurons (Ichida et al 2014). It is possible that macaque CG neurons display greater morphological variation compared to other species due to specializations of the Old World primate visual system, including high acuity and color vision. Alternatively, inconsistent findings on CG morphological diversity could be due to methodological variation. In most prior studies, selectively labeling CG neurons presented a substantial technical challenge, often yielding low sample sizes. Accordingly, direct comparison of CG neuronal morphology across primates and carnivores was limited, until now.

To explore CG morphological diversity across two species, we employed virus-mediated circuit tracing techniques to determine 1) whether CG neurons in ferrets display morphological diversity; and 2) whether morphologically distinct CG neuronal subtypes are similar across two highly visual species, ferrets and macaque monkeys. The current study of ferret CG morphology and the prior study of macaque CG morphology (Briggs et al 2016) both employed the same virus-mediated circuit tracing technique, which has a number of advantages over traditional retrograde tracing methods. Modified rabies virus is transported exclusively in the retrograde direction, is highly efficacious, and generates robust gene expression in infected neurons (Osakada et al 2011, Wickersham et al 2007). Robust infection and expression of fluorescent markers cause labeling of thousands of neurons per animal and enables resolution of unusual and/or rare neuronal types, which may be missed with conventional retrograde tracing methods (Callaway & Luo 2015). Additionally, fluorescent markers are expressed throughout the complete dendritic arborization of infected neurons, enabling accurate, complete, and high-throughput reconstructions of dendritic morphology followed by rigorous statistical analysis of morphological variation (Bragg & Briggs 2017, Briggs et al 2016).

We utilized the same experimental and data analysis strategies employed by Briggs et al (2016) to perform a thorough survey of CG neuronal morphology in ferrets. We reconstructed the full dendritic morphology of a large population of virus-labeled CG neurons in ferrets and observed three distinct morphological subtypes. Comparison of CG morphological subtypes in ferrets and macaques revealed striking similarities in dendritic arborization patterns. Together, these results support the notion that CG feedback is organized into parallel streams in at least two highly visual mammalian species.

MATERIALS AND METHODS

The tissue examined in this study was prepared as a part of a separate study (Hasse & Briggs 2017). All the experimental methods involving the use of animals were described in detail in the Materials and Methods and SI Appendix: Materials and Methods of Hasse and Briggs

(2017) and were approved by the Institutional Animal Care and Use Committee at Dartmouth. Detailed descriptions of the methods for stereotaxic injection of SAD-B19 rabies virus into the lateral geniculate nucleus (LGN), tissue harvesting, sectioning, staining, and reconstruction of labeled neurons were also described in detail previously (Bragg & Briggs 2017, Bragg et al 2017, Briggs et al 2016).

Virus-mediated neuroanatomical tracing

Genetically modified rabies virus: SADΔG-ChR2-mCherry or SADΔG-ArchT-GFP, both variants of SAD-B19 (Osakada et al 2011, Wickersham et al 2007), was injected into the LGN of 6 adult female ferrets (*Mustela putorius furo*) to label corticogeniculate (CG) neurons in layer 6 of visual cortical areas V1 and V2 (Brodmann areas 17 and 18). SADΔG-ChR2-mCherry and SADΔG-ArchT-GFP were taken up by axon terminals near the injection site, traveled retrogradely along axons to cell bodies, then replicated and expressed ChR2/mCherry or ArchT/GFP within infected CG neurons (Hasse & Briggs 2017). Importantly, SAD-B19 virus lacks the membrane-bound glycoprotein that enables the virus to cross synapses and infect new presynaptic neurons, therefore the virus remains restricted to the primarily infected neurons (Callaway 2009, Wickersham et al 2007). Neurons infected with virus express fluorescent proteins throughout their dendritic arbors, enabling complete reconstruction of dendritic morphology (see Figure 1). Virus-mediated delivery of fluorescent markers causes widespread labeling of individual neurons, making it possible to reconstruct large numbers of neurons including rare neuronal types (Bragg & Briggs 2017, Bragg et al 2017, Briggs et al 2016, Hasse & Briggs 2017). This high-throughput approach facilitates rigorous statistical analyses of distinct morphological subtypes within select neuronal populations.

Experimental procedures

Detailed descriptions of surgical methods, tissue sectioning, and staining have been described previously (Hasse & Briggs 2017). Briefly, surgical injections of rabies virus were conducted in a sterile surgical suite using aseptic techniques. A small craniotomy (<1 cm) was made and the location and depth of the LGN was neurophysiologically verified. Small amounts of virus (up to 5μL total) were injected at 4–5 different depths starting with the bottom of the LGN and moving dorsally ~200–500μm, with ~1000nL injected at each depth over 2–3 minutes using a nanoliter injector (Nanoject II; Drummond Scientific, Broomall, PA). Following surgery, animals recovered for 7 to 11 days to allow for maximal virus-mediated protein expression, after which a non-recovery experimental procedure was performed followed by euthanasia, perfusion, and brain tissue harvest. Tissue was frozen and blocks containing thalamus and visual cortex were sectioned coronally at a thickness of 70 μm using a freezing microtome (Thermo Scientific, Waltham, MA). LGN and cortical laminar boundaries were defined by cytochrome oxidase staining. Neurons were labeled with primary antibody against mCherry (rabbit anti-DS red, polyclonal, Clontech Laboratories Inc., Mountain View, CA, RRID: AB_10013483) or GFP (rabbit anti-GFP, polyclonal, Molecular Probes/Life Technologies, Grand Island, NY, RRID: AB_221570), followed by a biotinylated secondary antibody (goat anti-rabbit, Molecular Probes/Life Technologies, Grand Island, NY). Tissue was then reacted with DAB and peroxide to

permanently label infected CG neurons. Tissue sections were mounted on glass slides, dehydrated, defatted, and cover-slipped.

Reconstructing CG neurons in the visual cortex

We first verified that all neurons reconstructed in this population came from animals in which virus injections were within the LGN. In one animal (73014, see Hasse & Briggs, 2017, Supplemental Figure 1A), a large virus injection into the rostral and ventral portion of the LGN resulted in a small spread of virus below the LGN, possibly into the pulvinar complex (Yu et al 2016). In this animal, we observed 21 virus-labeled neurons in layer 5 of V1 that resembled large, Meynert-like neurons (le Gros Clark 1942, Winfield et al 1983). These neurons were restricted to two retinotopic regions within area 17 and made up a very small proportion of the total labeled neurons in areas 17 and 18 in this experimental animal (>3000 total labeled neurons). All the remaining labeled neurons were restricted to layer 6. We avoided the two retinotopic regions containing labeled neurons in layer 5 when we reconstructed virus-labeled layer 6 neurons in this animal. In the remaining 5 animals, there were no virus-labeled neurons outside of layer 6, consistent with prior studies demonstrating that CG neurons are restricted to layer 6 (Briggs et al 2016, Fitzpatrick et al 1994, Gilbert & Kelly 1975, Katz 1987).

We reconstructed the dendritic morphology of a total of 98 virus-infected layer 6 neurons in the visual cortex of 6 animals (range = 4–27 neurons per animal, mean = 16.3±4 neurons per animal, median = 17.5). We preferentially reconstructed neurons that were more isolated from neighboring labeled neurons to unambiguously assign dendritic processes to each reconstructed neuron. A Neurolucida system (MicroBrightField, Williston, VT; RRID: SCR_001775) with an Optronics camera attached to a Nikon E800M microscope (Nikon Instruments, Inc., Melville, NY) was used to trace contour and laminar boundaries, cell bodies, and dendritic arbors. LGN and injection site contours were traced for each animal to generate 3-D renderings of the injection sites (Supplemental Figure 1 of Hasse & Briggs 2017). We preferentially selected neurons for reconstruction that had cell bodies entirely contained within a single section to accurately estimate cell body area and roundness. We traced each dendritic process originating from the cell body placing nodes at each branch point and following dendritic processes through at least 3 adjacent tissue sections (at least one above and one below the section containing the cell body), up to a maximum of 5 adjacent sections. We were unable to trace axons of labeled CG neurons, as rabies virus does not reliably label CG axons (Briggs et al 2016).

Analysis of morphological data

The following morphological data were quantified from each CG reconstruction. Cell body position within layer 6 was measured as the proportional distance between the cell body and the contour marking the top of layer 6 compared to the extent of layer 6 (measured as the top of layer 6 to the white matter border centered around the location of the cell body). Maximum apical dendritic height was measured as the proportional distance between the top of the apical dendrite and the top of layer 1 compared to the full cortical depth (measured as the top of layer 1 to the white matter border). For stellate neurons, the top of the dendrite closest to the pia was used for an analogous measurement. Cell body size was computed as

the area of the cell body contour, drawn through the largest extent of the cell body within the home section containing the cell body. Cell body roundness was computed from the cell body contour. The angle at which the primary apical dendrite exited the cell body relative to a line tangential to the pial surface was recorded. For stellate neurons, which lack apical dendrites, the angle was recorded as zero. Proportions of basal dendrite in layers 5, 6, and in the white matter were computed by dividing basal dendrite per layer by the total basal dendrite. Proportions of apical dendrite in layers 2/3, 4, 5, and 6 were computed by dividing apical dendrite per layer by total apical dendrite. Proportions of basal and apical dendrite per layer were converted to percentages for display purposes. Finally, the total numbers of nodes and endings were recorded.

We applied an independent cluster analysis algorithm using all of the independent morphological metrics exported from each of the 98 CG reconstructions as the input. Because the cluster analysis algorithm assumes each parameter is independent (Bragg & Briggs 2017, Bragg et al 2017, Cauli et al 2000, Thorndike 1953) we excluded number of endings because this metric is not independent of number of nodes. The 13 parameters included in the cluster analysis were: cell body size, cell body roundness, number of nodes, proportion of basal dendrite in layers 5, 6, and the white matter, proportion of apical dendrite in layers 2/3, 4, 5, and 6, location of the cell body in layer 6, height of the apical dendrite (tallest point on stellate neurons), and the angle of the apical dendrite. Each of these 13 parameters were equally weighted in the cluster analysis. The Euclidean distance between each neuron, defined as a point in a 13-dimensional space, was computed using the “pdist” Matlab function (The Mathworks Inc., Natick, MA; RRID: SCR_001622). Clusters were defined by the inner squared distance between neurons using the “linkage” function (applying Ward’s method). The “dendrogram” function was used to visualize the linkage distances between neurons and illustrate clustering (Figure 2a).

Statistical verification of clustering

We used two different statistical methods to evaluate the clusters determined by the cluster analysis described above. First, we used statistical evaluation criterion outlined by the Calinski/Harabasz method (Calinski & Harabasz 1974) to test for the optimal cluster number out of 1 to 6 possible clusters. We used the “evalclusters” Matlab function to perform this test. The second statistical analysis we employed was a Gaussian mixture model (GMM) clustering algorithm (Talebi & Baker 2016). GMMs require a putative cluster number assignment. To avoid *a priori* assignment of number of clusters, we performed a principal component analysis (PCA) on all 13 morphological metrics within each GMM test, again testing for a putative number of clusters between 1 and 6. We used the PCA scores as the input to the “fitgmdist” Matlab function to test each GMM using three different evaluations: negative log likelihood, Akaike information criterion, and Bayes information criterion. The GMM with the lowest criteria across the three evaluations indicates the optimal number of clusters (Bragg & Briggs 2017).

Once the optimal cluster number was determined using the above statistical evaluations, we grouped morphological data for the 98 reconstructed CG neurons according to their cluster assignment. We then performed statistical evaluations of each morphological metric across

neurons in the clusters using non-parametric multiple-comparisons tests (Kruskal Wallis one-way ANOVA). Apical dendrite measurements (height, angle, and proportion per layer) were only compared across two clusters since Cluster 2 contained stellate neurons lacking apical dendrites. For statistical comparisons of these morphological metrics across neurons in two clusters, two-sample comparison tests (Wilcoxon rank-sum test) were used. Detailed statistics for all cluster comparisons are listed in Table 1.

RESULTS

The goals of this study were to generate complete dendritic morphological reconstructions of corticogeniculate (CG) neurons in areas 17 and 18 of ferret visual cortex and to compare morphologies of ferret CG neurons with those of macaque CG neurons described previously (Briggs et al 2016). To accomplish these goals, we injected G-deleted rabies virus variants SADΔG-ChR2-mCherry or SADΔG-ArchT-GFP (Osakada et al 2011) into the lateral geniculate nucleus (LGN) of 6 adult female ferrets, resulting in robust expression of ChR2/mCherry or ArchT/GFP in CG neurons within areas 17 and 18 of ferret visual cortex (Hasse & Briggs 2017). We reconstructed the complete dendritic morphology of 98 CG neurons spanning all retinotopic regions of areas 17 and 18.

Multiple CG subtypes in layer 6 of visual cortex revealed by retrograde virus infection

Virus-labeled CG neurons were restricted to layer 6 in visual cortical areas 17 and 18, corresponding to primary and secondary visual cortex (Briggs et al 2016, Hasse & Briggs 2017). Qualitative observations revealed multiple morphologically distinct neuronal subtypes within the virus-labeled CG population (Figure 1). In areas 17 and 18, we observed both short (n = 29) and tall (n = 29) pyramidal cells (Figure 1a1 & a2) resembling excitatory neuronal subtypes found in layer 6 of multiple mammalian species (Briggs et al 2016, Gilbert & Kelly 1975, Hirsch et al 1998, Katz 1987, Lund et al 1988, Lund et al 1979, Olsen et al 2012, Wiser & Callaway 1996, Zarrinpar & Callaway 2006). We identified tilted CG neurons with apical dendrites exiting cell bodies at near-90-degree angles (Figure 1a3; n = 7) in both areas 17 and 18. Tilted CG neurons in ferrets were strikingly similar to tilted CG neurons in macaque V1 and V2 (Briggs et al 2016). Additionally, spiny stellate neurons lacking apical dendrites were present in areas 17 and 18 (Figure 1a4; n = 24). Stellate CG neurons in ferrets were morphologically similar to layer 6 stellate neurons described previously (Prieto & Winer 1999, Tombol 1984, Zhang & Deschenes 1997) and to stellate CG neurons in macaques (Briggs et al 2016).

In area 18, we identified additional unusual and rare CG subtypes. Tall CG neurons with apical dendritic tufts (Figure 1b1 & b2; n = 3) were similar to large CG neurons in macaque V1 defined by larger cell bodies and apical dendrites extending to the pia where they branched to form tufts. Interestingly, macaque large CG neurons were observed in V1 while ferret tall-tufted CG neurons were observed in area 18. We observed a handful of displaced CG neurons in area 18 (Figure 1b4; n = 4), characterized by non-vertically oriented apical dendrites traveling horizontally within layer 6 or down into the white matter, as previously described (Prieto & Winer 1999, Tombol 1984). Finally, we observed a unique and potentially newly identified neuronal type, hereafter called a U-shaped cell (Figure 1b3; n =

1). This neuron had a very large cell body with two prominent apical dendrites curving away from the cell body and toward the pia, forming a “U” shape. The apical dendrites had tufts at the pial surface and the basal and apical dendrites closer to the cell body always extended outward in a symmetric manner. While it is possible that this rare CG type was a developmental mistake, its singular morphology and symmetrical arborization suggest a specific purpose.

Quantitative analysis revealed three clusters of CG neurons

A major advantage of virus-mediated circuit tracing is that large numbers of well-labeled neurons enable rigorous statistical analyses of morphological metrics (Bragg & Briggs 2017, Bragg et al 2017, Briggs et al 2016). The following morphological metrics were exported from each of the 98 CG reconstructions and utilized for quantitative analyses: cell body size, cell body roundness, cell body position in layer 6, number of dendritic nodes, proportion of basal dendrite in layers 5, 6, and white matter, proportion of apical dendrite in layers 2/3, 4, 5, and 6, height of apical dendrite, and angle of apical dendrite (see Materials and Methods). We performed an independent cluster analysis using all 13 of the independent morphological metrics listed above. Because the clustering algorithm assumes each parameter is independent (Bragg & Briggs 2017, Cauli et al 2000, Thorndike 1953), we excluded number of dendritic endings because this metric is not independent of number of nodes. Importantly, each of the 13 morphological metrics included in the cluster analysis were equally weighted. Figure 2a illustrates a dendrogram of the linkage distances between all 98 CG neurons, in which each neuron is color-coded according to the qualitative assignment of morphological type (short CG neurons in red, stellate CG neurons in purple, tall CG neurons in blue, tilted CG neurons in orange, unusual/rare CG neurons in green, as in Figure 1). The cluster analysis revealed three distinct clusters: Cluster 1 (n=43) contained almost all of the short CG neurons, most of the tilted CG neurons, and some unusual/rare CG neurons; Cluster 2 (n=25) contained all but two stellate CG and three short CG neurons; and Cluster 3 (n=30) contained all the tall CG neurons, two stellate CG neurons, and a handful of tilted and unusual CG neurons (Figure 2a).

To statistically evaluate the optimal number of clusters, we performed two independent tests of the cluster analysis based on all 13 morphological metrics. First, we applied the Calinski/Harabasz method (Calinski & Harabasz 1974) to evaluate the optimal cluster number testing from 1 to 6 possible clusters. This evaluation indicated that the optimal cluster number was 3. Second, we applied a Gaussian mixture model (GMM) clustering algorithm (Talebi & Baker 2016) to again evaluate the optimal cluster number testing from 1 to 6 possible clusters. To avoid *a priori* assumptions about cluster number, we performed principal components analysis (PCA) and used the PCA scores for each GMM test. We then evaluated each GMM test using three different assessments: negative log likelihood, Akaike information criterion, and Bayes information criterion. The GMM with the lowest criteria across the three evaluations indicated the optimal number of clusters (Bragg & Briggs 2017). All criteria reached minima for a cluster number of 3. Together, these analyses supported qualitative evaluation of the dendrogram (Figure 2a) indicating three distinct morphological subtypes of ferret CG neurons. Clear separation of neurons in each cluster (color coded by

cluster assignment in Figure 2a) was also apparent based on comparison of the first two principal component scores for each CG neuron (Figure 2b)

After determining the optimal number of clusters, we explored whether neurons in the three clusters differed along any of the 13 morphological metrics included in the cluster analysis. Since stellate CG neurons lacked apical dendrites, we excluded Cluster 2 from comparisons of metrics involving apical dendrites (proportion of apical dendrite in layers 2/3, 5, and 6, height of apical dendrite, angle of apical dendrite). The results of all comparisons, including detailed statistics, are listed in Table 1.

Figure 3 illustrates six comparisons across clusters that best distinguished the three CG morphological subtypes. Neurons in Clusters 1 and 3 differed significantly in both height of apical dendrite (Figure 3a, $P = 0.0183$) and percentage of apical dendrite in layer 2/3 (Figure 3b, $P = 4.9 \times 10^{-6}$), indicating that short (Cluster 1) and tall (Cluster 3) CG neurons formed distinct CG subtypes. Indeed, all Cluster 1 neurons lacked apical dendrites in layer 2/3 (Figure 3b), fitting the definition of short pyramidal neurons in layer 6 (Briggs 2010). Neurons in Cluster 3 also had significantly larger cell bodies relative to other CG neurons (Figure 3c, $P = 9.7 \times 10^{-15}$), likely because Cluster 3 contained tall-tufted CG neurons that were similar to large CG neurons in macaque V1 (Briggs et al 2016). Additionally, Cluster 1 contained the majority of the tilted CG neurons, which had smaller cell bodies (again similar to tilted CG neurons in macaque). Interestingly, neurons in Clusters 1 and 3 also differed significantly in the angle at which the apical dendrite exited the cell body. Apical dendrite angles were significantly larger for Cluster 1 neurons (Table 1, $P = 0.016$), due to the inclusion of tilted neurons in Cluster 1. Consistent with macaque CG subtypes, Cluster 1 CG neurons had more apical dendrite in layer 5 compared to Cluster 3 CG neurons (Figure 3d, $P = 0.004$), suggesting that short CG neurons have greater connectivity with layer 5 compared to tall CG neurons in both macaques and ferrets.

The most obvious difference between Cluster 2 neurons and CG neurons in Clusters 1 and 3 was the absence of apical dendrites among Cluster 2 neurons, the majority of which were stellate neurons. However, Cluster 2 neurons also differed from neurons in Clusters 1 and 3 in that their cell bodies were significantly deeper within layer 6 (Figure 3e, $P = 0.005$). Indeed, Cluster 2 neurons often had cell bodies in the white matter: 8 of 25 Cluster 2 neurons had cell bodies at or below the layer 6-white matter border (Figure 1a4). Accordingly, neurons in Cluster 2 had significantly less basal dendrite in layer 6 compared to Cluster 1 neurons (Figure 3f, $P = 0.0367$), likely because basal dendrites of Cluster 2 neurons were often in the white matter as well. In this regard, stellate CG neurons in ferret visual cortex differed from stellate CG neurons in macaque visual cortex: ferret stellate CG neurons were located deep in layer 6 while macaque stellate CG neurons were located in the upper third of layer 6 (Briggs et al 2016).

Similarities between CG subtypes in ferret and macaque visual cortex

When distinct CG subtypes from ferret (Figure 4a) and macaque (Figure 4b) visual cortex were compared side-by-side, numerous striking morphological similarities were apparent. Short (red), tall (blue), tilted (orange), and stellate (purple) CG neurons were morphologically similar across species based on overall arborization pattern, proportion of

dendrite per layer, and cell body size. Furthermore, short, tall, and tilted CG neurons were observed in both areas 17 and 18 in ferrets and in both V1 and V2 in macaques. The main difference in CG subtypes across ferrets and macaques was the sublaminar organization of cell bodies within layer 6. While macaque CG subtypes were segregated into upper or lower tiers of layer 6 (Briggs et al 2016, Fitzpatrick et al 1994), ferret CG neurons were distributed throughout layer 6, although short CG neurons tended toward the upper part of layer 6 while tall CG neurons were often deeper and stellate CG neurons were significantly deeper on average (Figure 3e). The lack of sublaminar segregation of ferret CG subtypes could reflect the fact that X and Y geniculocortical inputs to area 17 in carnivores are overlapping and distributed throughout layer 6 (Humphrey et al 1985a).

While spiny stellate CG neurons were present in both ferrets and macaques, there were some interesting differences across species. Stellate CG neurons were found in both areas 17 and 18 in ferrets, but only in V1 in macaques (Briggs et al 2016). Additionally, stellate CG neurons were located deeper in layer 6 in ferrets, while in macaques stellate CG neurons were always in the upper tier of layer 6 (Briggs et al 2016).

In macaques, the most unusual and rare CG subtypes were the large CG neurons with cell bodies in the upper tier of layer 6 and tall apical dendrites with tufts (Briggs et al 2016). Similar tall-tufted CG neurons were observed in area 18 in ferrets. In addition to the tall-tufted CG neurons, we observed displaced CG neurons and a single U-shaped CG in ferret area 18 (Figure 4a, **green**). Whether additional unusual and rare CG subtypes exist in both species remains to be discovered. Nevertheless, it is tempting to speculate that these more unusual CG subtypes in both species form the basis for feedback to the C and koniocellular layers within the LGN.

DISCUSSION

The advent of rabies virus-mediated circuit tracing techniques enabled thorough morphological surveys of identified populations of neurons. We harnessed these powerful tools to characterize the morphological diversity of CG neurons in the ferret and to compare ferret CG morphological subtypes to those described previously in macaque monkeys following application of the same virus-mediated tracing techniques (Briggs et al 2016). We previously demonstrated that G-deleted rabies virus selectively infects CG neurons in areas 17 and 18 (V1 and V2) in both ferrets and macaques following injection into the LGN (Briggs et al 2016, Hasse & Briggs 2017). In this study, we reconstructed the complete dendritic morphology of a large number of ferret CG neurons and employed quantitative analyses to define significant differences across CG morphological subtypes. Both qualitative (Figure 1) and quantitative (Figures 2, 3) assessments revealed three distinct clusters of ferret CG neurons distinguished based on 13 independent morphological metrics. Finally, we compared the morphological characteristics of ferret CG neurons with those of macaques (Figure 4). We noted several striking similarities across the two species, including similar general cellular structure and laminar location of dendritic arbors for CG neurons of each subtype. The only major difference between ferret and macaque CG subtypes was the organization of cell body position within layer 6. Together these results suggest that CG neurons are morphologically diverse in ferrets and macaques, consistent with the notion that

CG circuits are organized into functionally segregated parallel processing streams in at least two highly visual mammals.

In both ferrets and macaques, CG neurons fit broadly into three categories: short pyramidal, tall pyramidal, and stellate neurons. Two additional CG subtypes, tilted and large CG neurons were described in macaques and were also observed in ferrets. Short CG neurons (Cluster 1 neurons in ferrets, Iβ neurons in macaques; (Briggs & Callaway 2001, Briggs et al 2016, Wiser & Callaway 1996) were pyramidal cells with apical dendrites within and not above layer 4 (Figure 1a1). In both species, basal dendrites of short CG neurons were mostly restricted to layer 6 (Figure 3f and Briggs et al 2016, Figure 4A). Additionally, short CG neurons in both ferrets and macaques had more apical dendritic arbors in layer 5 compared to tall CG subtypes (Figure 3d and Briggs et al 2016, Figure 2B), suggesting short CG neurons may have greater local circuit interactions with neurons in layer 5. Iβ neurons in macaques displayed additional morphological characteristics indicating selective relationships with parvocellular stream neurons: Iβ cell bodies were restricted to the upper tier of layer 6, the termination zone of parvocellular geniculocortical afferents collaterals (Blasdel & Lund 1983, Fitzpatrick et al 1994, Hendrickson et al 1978, Hubel & Wiesel 1972) and Iβ apical dendrites targeted the parvocellular geniculocortical afferent sub-layer 4Cβ (Wiser & Callaway 1996). It is difficult to infer whether short CG neurons in ferrets are associated with the X stream because X and Y geniculocortical afferents in layer 4 and afferent collaterals in layer 6 are intermixed in carnivores (Humphrey et al 1985a). Thus even though ferrets CG neurons lack the strict sublaminar cell body organization seen in macaques, ferret CG neurons could maintain stream-specific relationships through specific afferent and local circuit connections.

Tall and tall-tufted CG neurons were included in Cluster 3. Tall CG neurons in ferret area 17 (Figure 1a2; Figure 3a–b) were similar to IC CG neurons in macaques (Briggs & Callaway 2001, Briggs et al 2016, Wiser & Callaway 1996). IC and tall CG neurons fit the generic definition of tall neurons in that they were pyramidal neurons with apical dendrites extending into layer 2/3. In both ferrets and macaques, IC/tall CG neurons had apical dendrites throughout layer 4. IC neurons showed no preferences for parvocellular or magnocellular termination zones in layer 4C (Wiser & Callaway 1996) and, like ferret tall CG neurons, had fewer apical dendrites in layer 5 compared to short CG neurons (Figure 3d). Based on functional local circuit connectivity and cell body position in the bottom tier of layer 6, the magnocellular geniculocortical afferent collateral termination zone, IC neurons had stronger relationships with the magnocellular stream (Briggs & Callaway 2001, Fitzpatrick et al 1994). Cell bodies of ferret tall CG neurons extended into deeper portions of layer 6, but displayed no obvious sublaminar organization. Nonetheless, tall CG neurons could maintain selective connectivity with neurons in the Y stream.

Although they clustered with tall CG neurons, tall-tufted CG neurons in ferret area 18 (Figures 1b1, 1 b2) were similar to large CG neurons in macaques. Both had large cell bodies and apical dendrites extending to the pia where they branched to form tufts. Large CG neurons and tall-tufted CG neurons could be affiliated with koniocellular and W streams, respectively. Based on their cell body position in the top tier of layer 6, large CG neurons in macaque V1 could project to the dorsal koniocellular LGN layers. Tall-tufted CG

neurons in ferret area 18 could project to the C LGN layer, consistent with results demonstrating that most feedback to the C layer originates in area 18 (Humphrey et al 1985b).

Stellate CG neurons (Figure 1a4; Cluster 2) had similar cellular morphology to stellate CG neurons in macaques, most notably lacking apical dendrites. While macaque stellate CG neurons were restricted to the top tier of layer 6, ferret stellate CG neurons were often positioned deep in layer 6 and in the white matter (Figure 3e). Additionally, stellate CG neurons were observed in both areas 17 and 18 in ferrets, but only in V1 in macaques. Given their unique and common cellular morphology, stellate CG neurons in both species may be functionally similar, perhaps projecting to koniocellular/C layers in the LGN.

Tilted CG neurons, first described in Briggs et al (2016), were also observed in ferret visual cortex (Figure 1a3). In both macaques and ferrets, tilted CG neurons were found in V1/area 17 and V2/area 18. Tilted CG cell bodies in both species were small and oval, not pyramidal. Most notably, the apical dendrites of tilted CG neurons exited the cell body from the side, then turned about 90 degrees and continued toward the pia. Again, the only difference between tilted CG neurons in macaques and ferrets was cell body position within layer 6. Macaque tilted cells are restricted to the lower tier of layer 6, while ferret tilted CG neurons showed no obvious sublaminar organization. Tilted CG neurons in macaques were hypothesized to be the slowly conducting, koniocellular projecting neurons described in Briggs & Usrey (2009). Similar slowly conducting CG neurons were also physiologically characterized in ferrets (Briggs & Usrey 2005), thus it is tempting to speculate that tilted CG neurons in both species are koniocellular/W stream feedback neurons with slowly conducting axons.

In this study, we included reconstructions from unusual CG neurons including displaced (Figure 1b4) and U-shaped neurons (Figure 1b3). It will be interesting to determine whether these unusual CG neuronal types are developmental mistakes in individual animals or specialized neurons serving a unique purpose. Additional comparative CG neuroanatomical studies would shed light on the prevalence and function of these exceptional CG neurons.

Because we performed a side-by-side comparison in which the same virus, experimental approach, clustering analyses, and statistical measures were employed, variations in CG morphology observed across species should be due to species differences and not experimental variation. Additionally, given the efficacy of virus-mediated circuit tracing at labeling broad samples of CG neurons, it was unlikely that employment of similar methods in two species would result in labeling of the same, limited subsample of neurons in both species. We discovered that ferret CG neurons were comprised of heterogeneous, distinct morphological subtypes that were markedly similar to the CG subtypes previously classified in macaques. Whether similar CG morphological diversity across these two species arose via evolution from a common ancestor, or arose via convergent evolution, remains to be tested. A thorough and targeted survey of CG neurons across a wide range of species spanning multiple phylogenetic branches could reveal the evolution of CG diversity.

If function follows form, then a primary functional role of diverse morphological CG subtypes could be the preservation of parallel information processing streams in the CG feedback pathway. Independent evidence in favor of parallel stream organization of CG feedback includes physiological measurements of identified CG neurons in macaques showing physiological response properties aligned with those of the feedforward streams (Briggs & Usrey 2009). In carnivores, multiple physiologically distinct CG subtypes have also been characterized (Briggs & Usrey 2005, Grieve & Sillito 1995, Harvey 1978, Tsumoto & Suda 1980). Finally, axonal termination patterns of CG neurons hint at stream-specific connectivity. Primate CG axons mainly terminate within single LGN layers (Ichida & Casagrande 2002, Ichida et al 2014). In carnivores, CG axons target A and A1 LGN layers, however X and Y neurons are intermixed within these LGN layers (Claps & Casagrande 1990, Erisir et al 1997a, Erisir et al 1997b, Murphy & Sillito 1996, Robson 1983). While a direct link between structure and function is still required to prove that CG feedback is organized into functionally stream-specific channels, similar morphological diversity of CG subtypes in ferrets and macaques supports this hypothesis. Future studies merging physiological and morphological analyses will help solve the enduring mystery of the functional organization of CG feedback.

Acknowledgments

Support: NIH/NEI EY018683 and EY025219, the Whitehall Foundation 2013-05-06, and the Albert J. Ryan Foundation

This work was funded by the NIH (NEI: EY018683 and EY025219), the Whitehall Foundation, and the Albert J. Ryan Foundation.

LITERATURE CITED

Andolina IM, Jones HE, Sillito AM. 2013; Effects of cortical feedback on the spatial properties of relay cells in the lateral geniculate nucleus. J Neurophysiology. 109:889–99.

Andolina IM, Jones HE, Wang W, Sillito AM. 2007; Corticothalamic feedback enhances stimulus response precision in the visual system. PNAS. 104:1685–90. [PubMed: 17237220]

Blasdel GG, Lund JS. 1983; Termination of afferent axons in macaque striate cortex. J Neurosci. 3:1389–413. [PubMed: 6864254]

Bragg EM, Briggs F. 2017; Large-scale reconstructions and independent, unbiased clustering based on morphological metrics to classify neurons in selective populations. Journal of Visualized Experiments. 120:1–10.

Bragg EM, Fairless EA, Liu S, Briggs F. 2017; Morphology of visual sector thalamic reticular neurons in the macaque monkey suggests retinotopically-specialized, parallel stream-mixed input to the lateral geniculate nucleus. Journal of Comparative Neurology. 525:1273–90. [PubMed: 27778378]

Briggs F. 2010; Organizing principles of cortical layer 6. Frontiers in Neural Circuits. 12:1–8.

Briggs F, Callaway EM. 2001; Layer-specific input to distinct cell types in layer 6 of monkey primary visual cortex. J Neurosci. 21:3600–08. [PubMed: 11331389]

Briggs F, Kiley CW, Callaway EM, Usrey WM. 2016; Morphological substrates for parallel streams of corticogeniculate feedback originating in both V1 and V2 of the macaque monkey. Neuron. 90:388–99. [PubMed: 27041497]

Briggs F, Usrey WM. 2005; Temporal properties of feedforward and feedback pathways between thalamus and visual cortex in the ferret. Thalamus and Related Systems. 3:133–39. [PubMed: 18176624]

Briggs F, Usrey WM. 2007; A fast, reciprocal pathway between the lateral geniculate nucleus and visual cortex in the macaque monkey. J Neurosci. 27:5431–36. [PubMed: 17507565]

Briggs F, Usrey WM. 2009; Parallel processing in the corticogeniculate pathway of the macaque monkey. Neuron. 62:135–46. [PubMed: 19376073]

Brumberg JC, Hamzei-Sichani F, Yuste R. 2003; Morphological and physiological characterization of layer 6 corticofugal neurons of mouse primary visual cortex. J Neurophys. 89:2854–67.

Calinski T, Harabasz J. 1974; A dendrite method for cluster analysis. Commun Stat Theory Methods. 3:1–27.

Callaway, EM. Cell types and local circuits in primary visual cortex of the macaque monkey. In: Chalupa, L, Werner, J, editorsThe Visual Neurosciences. Cambridge, MA: MIT Press; 2004. 680–94.

Callaway EM. 2009; Transneuronal circuit tracing with neurotropic viruses. Current Opinion in Neurobiology. 18:1–7.

Callaway EM, Luo L. 2015; Monosynaptic circuit tracing with glycoprotein-deleted rabies viruses. Journal of Neuroscience. 35:8979–85. [PubMed: 26085623]

Casagrande, VA, Xu, X. Parallel visual pathways: A comparative perspective. In: Chalupa, L, Werner, J, editorsThe Visual Neurosciences. Cambridge, MA: MIT Press; 2004. 494–506.

Cauli B, Porter JT, Tsuzuki K, Lambolez B, Rossier J, et al. 2000; Classification of fusiform neocortical interneurons based on unsupervised clustering. PNAS. 97:6144–49. [PubMed: 10823957]

Claps A, Casagrande VA. 1990; The distribution and morphology of corticogeniculate axons in ferrets. Brain Research. 530:126–29. [PubMed: 2271942]

Conley M, Raczkowski D. 1990; Sublaminar organization within layer 6 of the striate cortex in galago. J Comp Neurol. 302:425–36. [PubMed: 1705271]

Erisir A, Van Horn SC, Bickford ME, Sherman SM. 1997a; Immunocytochemistry and distribution of parabrachial terminals in the lateral geniculate nucleus of the cat: a comparison with corticogeniculate terminals. J Comp Neurol. 377:535–49. [PubMed: 9007191]

Erisir A, Van Horn SC, Sherman SM. 1997b; Relative numbers of cortical and brainstem inputs to the lateral geniculate nucleus. PNAS. 94:1517–20. [PubMed: 9037085]

Fitzpatrick D, Usrey WM, Schofield BR, Einstein G. 1994; The sublaminar organization of corticogeniculate neurons in layer 6 of macaque striate cortex. Visual Neurosci. 11:307–15.

Gilbert CD, Kelly JP. 1975; The projections of cells in different layers of the cat's visual cortex. J Comp Neurol. 163:81–106. [PubMed: 1159112]

Grieve KL, Sillito AM. 1995; Differential properties of cells in the feline primary visual cortex providing the corticofugal feedback to the lateral geniculate nucleus and visual claustrum. J Neurosci. 15:4868–74. [PubMed: 7623117]

Guillery RW. 1969; A quantitative study of synaptic interconnections in the dorsal lateral geniculate nucleus of the cat. Z Zellfrosch. 96:39–48.

Harvey AR. 1978; Characteristics of corticothalamic neurons in area 17 of the cat. Neuroscience Letters. 7:177–81. [PubMed: 19605109]

Hasse JM, Briggs F. 2017; Corticogeniculate feedback sharpens the temporal precision and spatial resolution of visual signals in the ferret. Proceedings of the National Academy of Science USA. 114:E6222–E30.

Hendrickson AE, Wilson JR, Ogren MP. 1978; The neuroanatomical organization of pathways between the dorsal lateral geniculate nucleus and visual cortex in the old world and new world primates. J Comp Neurol. 182:123–36. [PubMed: 100530]

Hirsch JA, Gallagher CA, Alonso J-M, Martinez LM. 1998; Ascending projections of simple and complex cells in layer 6 of the cat striate cortex. J Neurosci. 18:8086–94. [PubMed: 9742175]

Hubel DH, Wiesel TN. 1972; Laminar and columnar distribution of geniculo-cortical fibers in the macaque monkey. J Comp Neurol. 146:421–50. [PubMed: 4117368]

Humphrey AL, Sur M, Uhlrich DJ, Sherman SM. 1985a; Projection patterns of individual X- and Y-cell axons from the lateral geniculate nucleus to cortical area 17 in the cat. Journal of Comparative Neurology. 233:159–89. [PubMed: 3973100]

Humphrey AL, Sur M, Uhlrich DJ, Sherman SM. 1985b; Termination patterns of individual X- and Y-cell axons in the visual cortex of the cat: projections to area 18, to the 17/18 border region, and to both areas 17 and 18. Journal of Comparative Neurology. 233:190–212. [PubMed: 3973101]

Ichida JM, Casagrande VA. 2002; Organization of the feedback pathway from striate cortex (V1) to the lateral geniculate nucleus (LGN) in the owl monkey (aotus trivirgatus). J Comp Neurol. 454:272, 83. [PubMed: 12442318]

Ichida JM, Mavity-Hudson JA, Casagrande VA. 2014; Distinct patterns of corticogeniculate feedback to different layers of the lateral geniculate nucleus. Eye and Brain. 6:57–73.

Jackson CA, Hickey TL. 1985; Use of ferrets in studies of the visual system. Lab Animal Science. 35:211–15.

Jiang Z, Johnson R, Burkhalter A. 1993; Visualization of dendritic morphology of cortical projection neurons by retrograde axonal tracing. J Neurosci Methods. 50:45–60. [PubMed: 7506340]

Jones, EG. The Thalamus. New York, NY: Plenum Press; 1985.

Kaplan, E. The M, P, and K pathways of the primate visual system. In: Chalupa, L, Werner, J, editorsThe Visual Neurosciences. Cambridge, MA: MIT Press; 2004. 481–93.

Katz LC. 1987; Local circuitry of identified projection neurons in cat visual cortex brain slices. J Neurosci. 7:1223–49. [PubMed: 3553446]

le Gros Clark WE. 1942; The cells of Meynert in the visual cortex of the monkey. Journal of Anatomy. 76:369–76. [PubMed: 17104906]

Lin CS, Kaas JH. 1977; Projections from cortical visual areas 17, 18, and MT onto the dorsal lateral geniculate nucleus in owl monkeys. J Comparative Neurology. 173:457–74.

Lund JS, Hawken MJ, Parker AJ. 1988; Local circuit neurons of macaque monkey striate cortex: II. neurons of laminae 5B and 6. J Comp Neurol. 276:1–29. [PubMed: 2461395]

Lund JS, Henry GH, MacQueen CL, Harvey AR. 1979; Anatomical organization of the primary visual cortex (area 17) of the cat: a comparison with area 17 of the macaque monkey. J Comp Neurol. 184:599–618. [PubMed: 106072]

Murphy PC, Duckett SG, Sillito AM. 2000; Comparison of the laminar distribution of input from areas 17 and 18 of the visual cortex to the lateral geniculate nucleus of the cat. J Neurosci. 20:845–53. [PubMed: 10632614]

Murphy PC, Sillito AM. 1996; Functional morphology of the feedback pathway from area 17 of the cat visual cortex to the lateral geniculate nucleus. J Neuroscience. 16:1180–92.

Olsen SR, Bortone DS, Adesnik H, Scanziani M. 2012Gain control by layer six in cortical circuits of vision. Nature. :47–52.

Osakada F, Mori T, Cetin A, Marshel JH, Virgen B, Callaway EM. 2011; New rabies virus varients for monitoring and manipulating activity and gene expression in defined neural circuits. Neuron. 71:617–31. [PubMed: 21867879]

Prieto J, Winer J. 1999; Layer 6 in cat primary auditory cortex: golgi study and sublaminar origins of projection neurons. J Comp Neurol. 404:332–58. [PubMed: 9952352]

Robson JA. 1983; The morphology of corticofugal axons to the dorsal lateral geniculate nucleus in the cat. J Comp Neurol. 216:89–103. [PubMed: 6863597]

Sherman, SM, Guillery, RW. Exploring the thalamus and its role in cortical function. Boston: MIT Press; 2006.

Talebi V, Baker CI. 2016; Categorically distinct types of receptive fields in early visual cortex. Journal of Neurophysiology. 115:2556–76. [PubMed: 26936978]

Thorndike RL. 1953; Who belongs in the family? Psychometrika. 18:267–76.

Tombol, T. Layer VI cells. In: Peters, A, Jones, EG, editorsCerebral Cortex. New York: Plenum Press; 1984. 479–519.

Tsumoto T, Suda K. 1980; Three groups of cortico-geniculate neurons and their distribution in binocular and monocular segments of cat striate cortex. J Comp Neurol. 193:223–36. [PubMed: 7430428]

Updyke BV. 1975; The patterns of projection of cortical areas 17, 18, and 19 onto the laminae of the dorsal lateral geniculate nucleus in the cat. Journal of Comparative Neurology. 163:377–96. [PubMed: 1176644]

Usrey WM, Fitzpatrick D. 1996; Specificity in the axonal connections of layer 6 neurons in tree shrew striate cortex: evidence for distinct granular and supragranular systems. J Neurosci. 16:1203–18. [PubMed: 8558249]

Wickersham IR, Finke S, Conzelmann KK, Callaway EM. 2007; Retrograde neuronal tracing with a deletion-mutant rabies virus. Nature Methods. 4:47–49. [PubMed: 17179932]

Winfield DA, Neal JW, Powell TP. 1983; The basal dendrites of Meynert cells in the striate cortex of the monkey. Proc R Soc Lond Biol Sci. 217:129–39. [PubMed: 6188164]

Wiser AK, Callaway EM. 1996; Contributions of individual layer 6 pyramidal neurons to local circuitry in macaque primary visual cortex. J Neurosci. 16:2724–39. [PubMed: 8786448]

Yu C, Sellers KK, Radtke-Schuller S, Lu J, Xing L, et al. 2016; Structural and functional connectivity between the lateral posterior-pulvinar complex and primary visual cortex in the ferret. European Journal of Neuroscience. 43:230–44. [PubMed: 26505737]

Zarrinpar A, Callaway EM. 2006; Local connections to specific types of layer 6 neurons in the rat visual cortex. J Neurophysiology. 95:1751–61.

Zhang Z, Deschenes M. 1997; Intracortical axonal projections of lamina V1 cells of the primary somatosensory cortex in the rat: a single-cell labeling study. J Neurosci. 17:6365–79. [PubMed: 9236245]

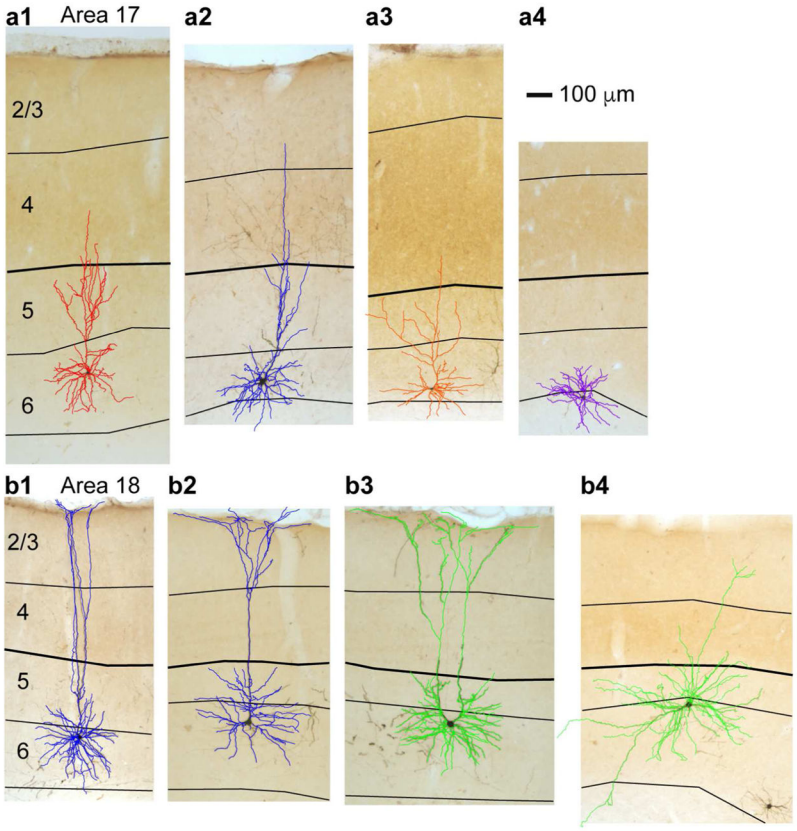

Figure 1. Dendritic reconstructions of representative CG neurons in areas 17 and 18 of ferret visual cortex

a and **b**. Photographs of virus-labeled CG neurons in cytochrome oxidase-stained coronal sections through areas 17 (**a**) and 18 (**b**) of ferret visual cortex. Reconstructions are overlaid and are colored according to qualitative assignment of morphological type: short in red, tall in blue, tilted in orange, stellate in purple, unusual/rare (displaced, U-shaped) in green. Short (**a1**), tall (**a2**), tilted (**a3**), and stellate (**a4**) CG neurons in area 17 and tall-tufted (**b1** and **b2**), U-shaped (**b3**), and displaced (**b4**) CG neurons in area 18 are displayed. Scale bar in **a4** represents 100μm and applies to all photograms and reconstructions. Black contours indicate layer boundaries, labeled on the left, and the layer 4/5 border is thickened in each image for continuity.

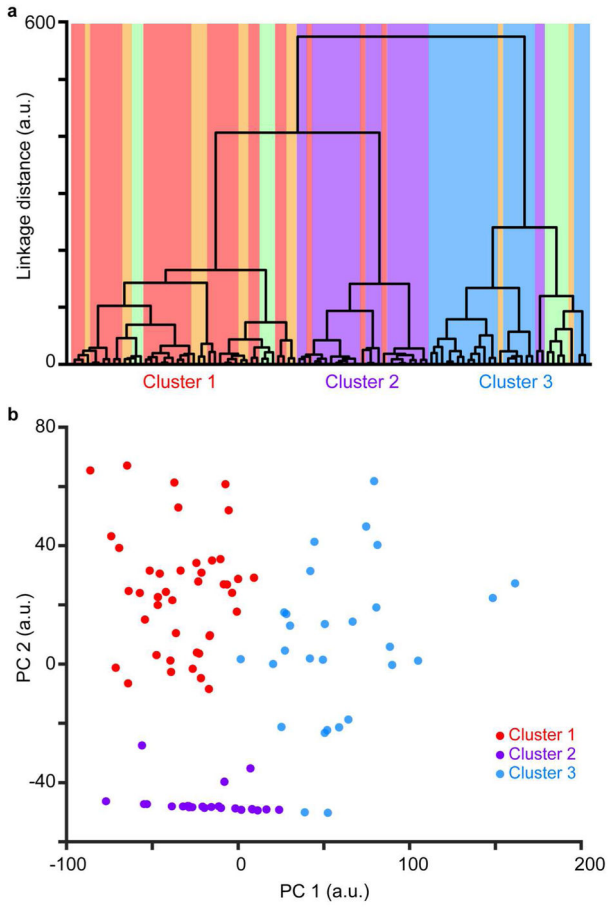

Figure 2. Quantitative analyses reveal 3 distinct clusters of ferret CG neurons

a. Dendrogram illustrating linkage distances between 98 CG neurons and three clusters (labeled on x-axis). Neurons (vertical bars) are colored according to qualitative assignment of morphological type: short, stellate, tall, tilted, and unusual/rare (displaced and U-shaped) CG neurons in red, purple, blue, orange, and green, respectively. **b**. Comparison of first and second principal component scores per CG neuron. PCA scores were generated from analysis of the same 13 morphological metrics used in the cluster analysis. Neurons are colored according to the primary color cluster assigned in **a**.

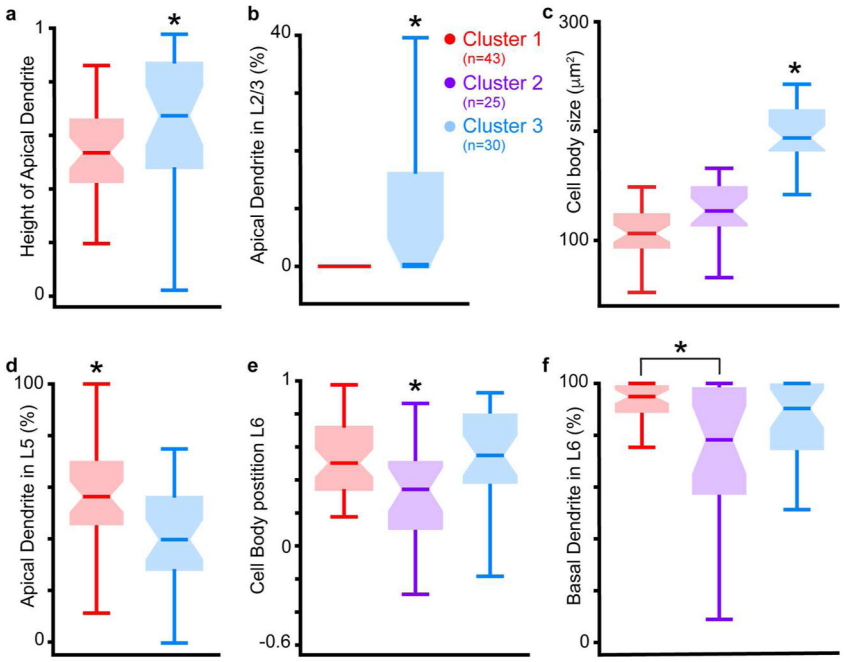

Figure 3. Differences in morphological metrics across clusters

a. Comparison of height of apical dendrite, as a proportion of the total cortical depth, across neurons in Clusters 1 and 3. Zero is white matter border, 1 is pial surface. Box plots illustrate median (horizontal bars) and variance (error bars) for neurons in each cluster, colored according to primary cluster assignment from Figure 2a (legend between **b** & **c**; numbers of neurons per cluster indicated in legend). Asterisk indicates significant differences across clusters (see Table 1 for detailed statistics). **b**. Comparison of percent of apical dendrite in layer 2/3 across neurons in Clusters 1 and 3. Conventions as in **a. c**. Comparison of cell body size across neurons in all three clusters, conventions as in **a** & **b. d**. Comparison of percent of apical dendrite in layer 5 across neurons in Clusters 1 and 3, conventions as in **a–c. e**. Comparison of cell body position in layer 6, proportional to the total depth of layer 6, across neurons in all clusters. Zero is white matter border, 1 is layer 5/6 border. Conventions as in **a–d. f**. Comparison of percent of basal dendrite in layer 6 across neurons in all clusters, conventions as in **a–e**.

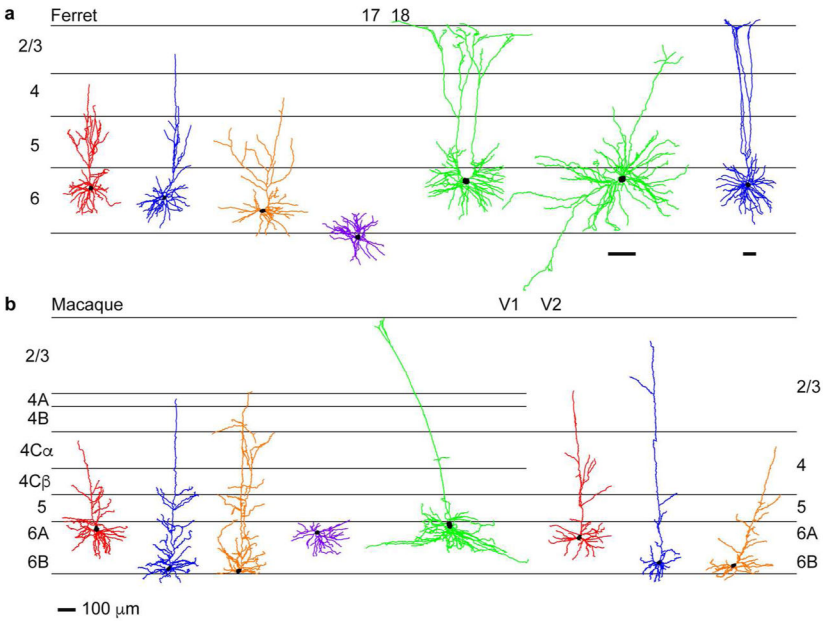

Figure 4. Morphological heterogeneity among CG neurons in ferret and macaque

a. Representative CG neurons of differing morphological subtype in ferret visual cortical areas 17 and 18 (cortical area boundary indicated at top, laminar boundaries indicated by black horizontal lines and labeled at left). Short, tall, tilted, stellate, and unusual morphological subtypes are indicated by red, blue, orange, purple, and green-colored dendritic reconstructions, respectively. Scale bar at the bottom of **b** represents 100μm and corresponds to all reconstructions in the figure except the top rightmost two reconstructions that have their own scale bars underneath, also representing 100μm. **b**. Representative CG neurons of differing morphological subtype in macaque visual cortical areas V1 and V2. Conventions and color-coding as in **a,** with V2 layer labeling at right. Reconstructions adapted from Figures 3 & 6 of Briggs et al (2016).

J Comp Neurol. Author manuscript; available in PMC 2020 February 15.

Table 1

Statistical comparison for 13 morphological metrics across Clusters 1, 2, and 3

	Cell Body Area (μm^2)	Cell Body Roundness	Number of Nodes	Cell Body Position in Layer 6 (prop. layer depth)	AD* Height (prop. cortical depth)	AD Angle (°)
Cluster 1 n= 43 Mean±SEM	107 ± 3.59	0.633 ± 0.0182	29.4 ± 1.03	0.531 ± 0.0343	0.549 ± 0.0265	71.3 ± 3.12
Cluster 2 n= 25 Mean±SEM	127 ± 5.26	0.692 ± 0.0192	25.2 ± 1.14	0.297 ± 0.0695	n/a	n/a
Cluster 3 n= 30 Mean±SEM	203 ± 6.55	0.69 ± 0.0186	35.2 ± 2.51	0.549 ± 0.0502	0.673 ± 0.0455	55.9 ± 4.96
P Value	9.7×10^{-15}	0.0461	0.0025	0.005	0.0183	0.0157
Cluster Differences	3 > 1 & 2	no diff	3 > 2	1 & 3 > 2	3 > 1	1 > 3

	BD* in Layer 5 (% total BD)	BD in Layer 6 (% total BD)	BD in White Matter (% total BD)	AD in Layer 2/3 (% total AD)	AD in Layer 4 (% total AD)	AD in Layer 5 (% total AD)	AD in Layer 6 (% total AD)
Cluster 1 n= 45 Mean±SEM	5.83 ± 2.48	90.9 ± 2.44	3.28 ± 0.781	0.108 ± 0.0751	9.41 ± 1.34	55.5 ± 3.37	34.9 ± 3.87
Cluster 2 n= 25 Mean±SEM	10.6 ± 3.6	73.5 ± 5.60	15.9 ± 5.28	n/a	n/a	n/a	n/a
Cluster 3 n= 30 Mean±SEM	10.6 ± 4.41	78.3 ± 5.38	10.3 ± 3.96	8.49 ± 2.38	13.0 ± 2.01	41.3 ± 3.71	29.7 ± 4.08
P Value	0.4502	0.0367	0.1348	4.9×10^{-6}	0.1757	0.004	0.3787
Cluster Differences	no diff	1 > 2	no diff	3 > 1	no diff	1 > 3	no diff

*AD = Apical dendrite; BD = Basal dendrite